Conformation Control of Model Peptides by Metal Ions. A New Type of Turn Structure Found in [(Boc–Cys–Pro–Leu–Cys–Gly–Ala)Hg]

Takeshi Yamamura,* Masaya Arai, Tsutomu Yamane, Takeshi Ukai, Masato Ushiyama, and Hiroshi Hirota†

Department of Chemistry, Faculty of Science, Science University of Tokyo, Kagurazaka, Shinjuku-ku, Tokyo 162

†Fusetani Biofouling Project, ERATO, JRDC, c/o Niigata Engineering Co., Ltd., 27 Shin-isogo-chou, Isogo-ku, Yokohama 235

(Received April 22, 1996)

The structure of [(Boc–Cys^1–Pro–Leu–Cys^4–Gly–Ala–OMe)Hg], **1**, in DMF($-d_7$) and DMSO($-d_6$) solutions was studied by X-ray absorption fine structure (XAFS), rotating frame nuclear Overhauser effect spectroscopy (ROESY), distance geometry (DG), molecular dynamics (MD), and restrained molecular dynamics (RMD). The XAFS study clarified that the inorganic center of compound **1** adopts a linear coordination with r(HG–S) = 2.33 Å. The NMR experiment revealed 33 atom approximate distances for the ^{1}H-^{1}H pairs of the main chain loop, including the side chains of the cysteinyl residues (ROESY). By a complementary use of DG, plain MD, and RMD for distance information from NMR as well as XAFS, we established that compound **1** adopts a new type of hybridized turn structure. The compound has two hydrogen bonds, Cys^1 S-Leu H_N and Pro CO-Cys^4 H_N, among which the former is common to the core sites in proteins, Cys^i–X–Y–Cys^{i+3}/M^{2+} (Zn^{2+}, Fe^{2+}), whereas the latter is common to the mirror image of the γ turn structure in proteins.

In the course of pursuing the principles of protein conformation, several basic types of turn structures have been proposed.[1] Among the turn structures, Cys^1–X–Y–Cys^4–A–B occupies a notable situation because of its ability to bind metal ions,[2—11] metal sulfide clusters,[12—17] and heme prosthetic groups,[18] as well as to form disulfide bridges.[19] This metal binding sequence is widely observed in such proteins as rubredoxins,[2] ferredoxins,[2] alcohol dehydrogenases,[3] zinc finger motifs,[4] metallothioneins,[5] and their regulatory proteins.[6] From the view point of structural chemistry with respect to bioinorganic chemistry, it is important that the local conformations of the sequences in the metal binding sites of these proteins seem to be predominated by the coordination geometries of the inorganic units (Fe^{2+},[7] Zn^{2+},[8—11] and Fe–S clusters[12—17]). Figure 1a is a schematic drawing of the Rub core site, which represents the Cys–X–Y–Cys combined with tetrahedral metal ions.[7—11] However, the details concerning the regulation by metal ions have remained unknown.

The introduction of inorganic center with abiological geometries into the small model pertides, including Cys^1–X–Y–Cys^4–A–B, may provide a new type of turn structures; a comparative study of such structures with those of the core sites in metallo proteins would reveal details concerning the conformational regulation of peptide chains by inorganic centers free from protein folding.

In a previous paper, we discussed the structure of [(Boc–Cys^1–Pro–Leu–Cys^4–OMe)Hg], **2** (Fig. 1d),[20] as well

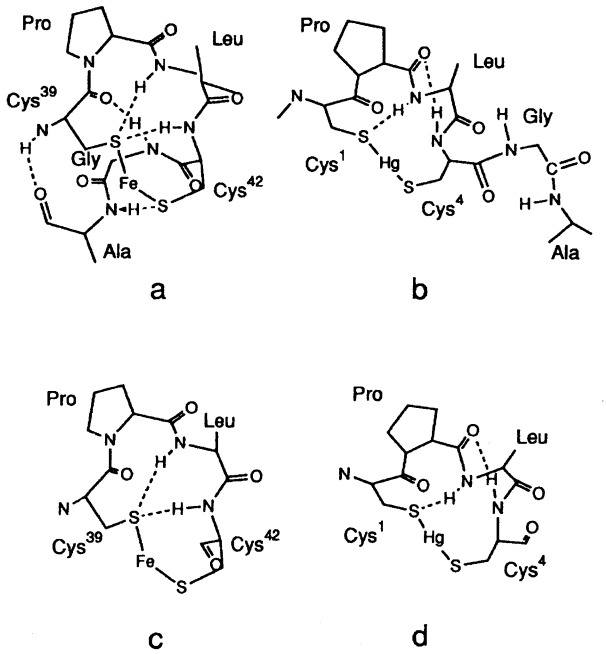

Fig. 1. Schematic structures of Cys^i–Pro–Leu– Cys^{i+3}/M^{2+}. (a) Cys^1–Pro–Leu–Cys^4/Hg^{2+},[20] (b) Cys^i–Pro–Val–Cys^{i+3}/M^{2+} (M = Fe, Zn) in metallo proteins.[5,7—11] (c) Cys^1–Pro–Leu–Cys^4–Gly–Ala/Hg^{2+}, (d) Cys^i–Pro–Val–Cys^{i+3}–Gly–Ala/M^{2+} (M = Fe, Zn) in metallo proteins.

as the effect of Hg^{2+} as a representative of linear coordination on the conformation of the Cys^1–Pro–Leu–Cys^4 sequence. However, the report was insufficient from the view point of establishing a new type of turn structure. The report was not able to clarify the hydrogen bonding character of Cys^4 H_N experimentally, and hence, failed to confirm the partner. The failure to observe the hydrogen bond character of this amide proton is attributed to the exposure of the amide to the solvent. Thus, in order to protect the Cys^4 H_N from access of the solvents, and thereby corroborating the hydrogen bonding, as well as to discuss the effect of peptide elongation on the conformation of Cys^1–Pro–Leu–Cys^4/Hg^{2+}, we prepared [(Boc–Cys^1–Pro–Leu–Cys^4–Gly–Ala–OMe)-Hg], **1**. We studied the structure of this compound in DMF($-d_7$) by X-ray absorption fine structure (XAFS),[21] nuclear Overhauser enhancement and exchange spectroscopy (NOESY),[22] molecular dynamics (MD),[23] restrained molecular dynamics (RMD),[24] and a distance geometry (DG) technique.[25] By this study, we revealed that the linear coordinate Hg^{2+} regulates Cys^1–Pro–Leu–Cys^4 to form a new type of turn structure, which is shown in Fig. 1b.

Experimental

Materials. The starting materials (Boc–Cys(Acm)–OH (Acm: acetamidemethyl; the protecting group of the sulfur), Boc–Pro–OH, Boc–Leu–OH, Boc–Gly–OH, and Boc–Ala–OH, as well as the coupling reagents for peptide synthesis, di-*t*-butyl dicarbonate (Boc_2O), 1-ethyl-3-(3-dimethylaminopropyl) carbodiimide hydrochloride (EDC), and 1-hydroxybenzotriazole (HOBt)) were obtained from Peptide Institute Inc. (Japan). Cys(Acm)–OMe was prepared according to the method of Walter et al.[26] All of the intermediates were purified on silica-gel columns, and the purities were checked by high-performance liquid chromatography (HPLC) (Shimadzu LC-6A/SPD-6A/C-R6A system with Shimpack ODS and ODP columns, Waters Model 510/Lambda-Max Model-481 with a Shimadzu PREP ODS and ODP columns, ϕ20×250 mm). They were identified by ^{1}H NMR (JEOL JNM-EX270). The hexamer peptide, Boc–Cys(Acm)–Pro–Leu–Cys-(Acm)–Gly–Ala–OMe, **3**, which is the precursor to compound **1**, was prepared from Boc–Cys(Acm)–Pro–Leu–Cys(Acm)–OMe[20] and Gly–Ala–OMe via the azide method. The crude compound was purified on a Sephadex LH 20 column using MeOH as an eluent. The final identification was performed by mass spectroscopy (Hitachi double-focusing FD mass spectrometer M-80), NMR, and elemental analysis.[27] [(Boc–Cys^1–Pro–Leu–Cys^4–Gly–Ala–OMe)-Hg], **1**, was prepared from compound **3** and $HgCl_2$, as described below, referring to the method of Ueyama et al.[28] and Yamamura et al.[20]

Deuterated solvents for NMR experiments ($CDCl_3$ (99.6%), DMSO-d_6 (99.96%), and DMF-d_7 (99.5%)) were purchased from Aldrich Inc.

[(Boc–Cys^1–Pro–Leu–Cys^4–Gly–Ala–OMe)Hg], 1.[29] Compound **3** (111.5 mg; 0.136 mmol) was dispersed in a least amount of DMSO (0.25 mL), into which was slowly added a DMSO (2.23 mL) solution of $HgCl_2$ (736.4 mg; 2.71 mmol) over 30 min. The mixture was stirred for 16 h, and then poured into ice water saturated with NaCl. The resulting white precipitate was quickly collected by filtration or centrifugation, subsequently washed with 5 ml of cold NaCl aq solution and 4 ml of ice water, then dried in vacuo. The material thus obtained was dissolved in MeOH, filtered through a membrane filter (ADVANTEC DISMIC-25 JP PTFE 0.20 μm) and purified on a gel chromatography column (Sephadex LH-20, ϕ30×*l*1000 mm, eluent MeOH). A fraction of more than 97% purity was collected and subjected to recrystallization from MeOH/Et_2O. This achieved a final purity of > 99.9% (HPLC). The yield was 60.4 mg (51.1%).

XAFS Experiment. Hg L(III) edge X-ray absorption was measured using the EXAFS facility of beam line BL-10B of the Photon Factory[30] at the National Institute of High Energy Physics (KEK) at Tsukuba. A Si(311) channel-cut, double-crystal monochromator was used. The measurements of the X-ray absorption near-edge structure (XANES) and extended X-ray absorption fine structure-(EXAFS) spectra of compound **1** were performed in the transmission mode at room temperature. The data were acquired using a 5 mm optical-path length cell with thin polyethylene windows. The concentration of the sample solution was controlled to be approximately the same as that for NMR (0.12 M; 49 mg/0.45 mL of DMF-d_7) for consistency.

XAFS analyses were performed according to the conventional method, described elsewhere.[20,21,31] The raw spectra observed in energy space (electronvolts) were reduced to the raw EXAFS function in the photoelectron wave vector (k) using the equation $k = [2m(E-E_0)/h^2]^{1/2}$ (E_0: the threshold energy), where the contributions from the preedge regions were approximated using Victoreen's function plus constants,[32] and the atomiclike backgrounds were determined by the cubic-spline method. Fourier transformations (FT) of the EXAFS signals to the radial distribution functions and their back FT were carried out using Hanning window with 1/20 of the FT ranges. The coordination number and the Hg–S distance for the first shell were derived by both curve fitting and a ratio method[33] based on the single scattering model,[34] where the experimental phase shifts (σ) and scattering amplitudes extracted from $[Hg(SCH_3)_2]$, $(NEt_4)[Hg(S\text{-}t\text{-}C_4H_9)_3]$, and $(NEt_4)_2[Hg(SC_6H_4Cl)_4]$were used.[20] The result was further simulated and confirmed by FEFF 6.01, the ab initio EXAFS standard developed by Rehr and his co-workers.[35] to take into account the multiple-scattering effect.

NMR. NMR data for ^{1}H and ^{13}C assignments (^{1}H-^{1}H COSY, ^{1}H-^{13}C COSY, DEPT (90°, 135°)) were collected with a BRUKER ARX500 spectrometer. A temperature-dependent ^{1}H NMR experiment was also carried out. A heteronuclear multiple-bond correlation (HMBC)[36] and phase-sensitive (PS) NOESY spectra were also measured. The PS NOESY and ROESY[37] data were acquired at 298 K using a mixing time (τ_m) of 0.6 s in the absorption mode with TPPI.[38]

Experimental Results

XAFS. The Hg L(III) edge XANES spectrum of compound **1** in DMF was at first compared with those of references having different types of HgS_n geometries: $[Hg(SCH_3)_2]$, linear;[39] $(NEt_4)[Hg(S\text{-}t\text{-}C_4H_9)_3]$, trigonal planar;[40] $(NEt_4)_2[Hg(SC_6H_4Cl)_4]$, tetrahedral.[41] The XANES spectrum of compound **1** was almost superimposed on that of a linear compound, $[Hg(SCH_3)_2]$, but not on those of the trigonal planar and tetrahedral compounds. A detailed comparison of the spectrum with those of other reference compounds has eventually suggested that compound **1** adopts a linear coordinate Hg^{2+} similarly to compound **2**. The Hg L(III) XANES spectrum of compound **1** in DMSO showed a similar result, but with bad quality because of the X-ray absorption by the sulfur atom of the solvent.

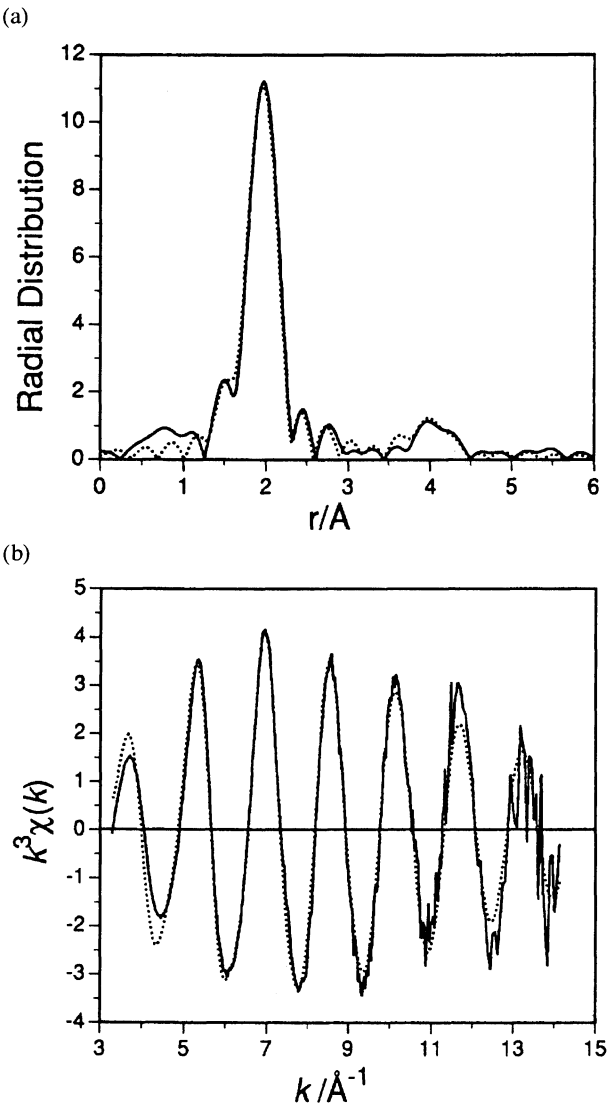

Fig. 2. (a, top) Fourier transforms of the Hg L(III) EXAFS of compound **1**. Solid line: the radial distribution function obtained by the Fourier transform of the raw EXAFS function (k=3.2—14.2 Å^{-1}). Dashed line: the theoretical curve obtained by the FT of the EXAFS function calculated by FEFF 6.01.[35] (b, bottom) EXAFS functions of the Hg L(III) EXAFS of compound **1**. Solid line: the raw EXAFS function of compound **1**. Dashed line: the theoretical EXAFS function obtained from the FEFF calculation. See Table 1 for the conditions of the calculation.

FT of the Hg L(III) EXAFS of compound **1** in DMF (Fig. 2a; solid line) shows a large radial distribution at about 2 Å. This peak originates from backscattering due to the sulfur atoms bound to Hg, whereas the small peaks around 4 Å originate from the multiple-scattering paths of the photoelectron, as will be shown later.

Table 1 summarizes the result of the EXAFS analysis for the first shell. The best fit was obtained from the parameters for $(NEt_4)[Hg(S\text{-}t\text{-}C_4H_9)_3]$ (No 2 in Table 1). Table 1 shows that Hg^{2+} has two sulfur atoms with r(Hg–S) = 2.33 Å. This is in good agreement with a previous result for compound **2** (2.33 Å), as well as that for the linear $[Hg(SCH_3)_2]$ (2.36 Å)

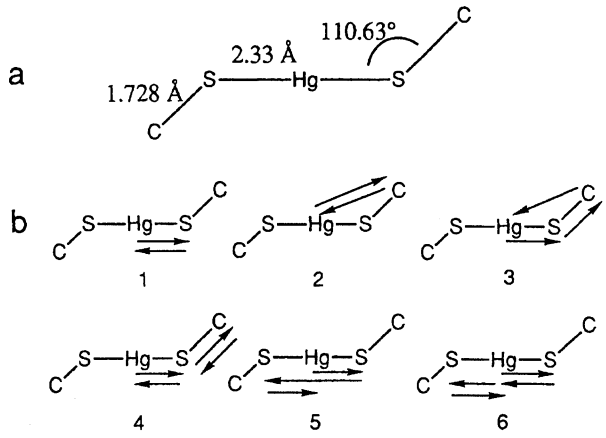

Fig. 3. (a) The $Hg(SC)_2$ core used for the FEFF calculation. (b) The dominant scattering paths calculated by FEFF 6.01[35] (see Table 1 for the conditions of the calculation, and Table 2 for the details of the scattering paths). The numbering of this figure corresponds to that of Table 2.

from X-ray crystallography.[39]

On the basis of these results, we generated theoretical χ data for compound **1** using FEFF 6.01 to simulate the raw EXAFS function and its FT (the solid lines in Figs. 2a and 2b. The values, r(Hg–S) = 2.33 Å, r(S–C) = 1.728 Å, and $\angle$(Hg–S–C) = 110.63°, for the $Hg(SC)_2$ core (Fig. 3a) were derived from the results of the EXAFS analysis described above with reference to the molecular structure of $[Hg(SCH_3)_2]$ by X-ray analysis.[39] Both the raw EXAFS function and its FT were best explained by assuming σ(Debye–Waller-like factor) = 0.061 Å, as corresponding to Θ_D (Debye temperature) = 575 K,[42] T = 295 K, and SO^2 (core hole reduction factor) = 0.85.[43] The contribution from multiple-scattering paths larger than 4.66 Å was negligible. The dashed lines in Fig. 2 exhibit the result of this best-fit calculation. These figures show that the FEFF calculation well reproduces the experimental results. The multiple-scattering paths calculated by FEFF 6.01 are summarized in Fig. 3b and Table 2.

NMR. All of the ^1H and ^{13}C NMR bands of compound **1**, except for the pro-chiral protons of Cys^1 H_β, Pro $H_{\beta,\delta}$, and Cys^4 H_β, were assigned by DEPT, ^1H- ^1H, ^1H-^{13}C COSY, Inv. 4TP and HMBC for both the DMF-d_7 and DMSO-d_6 solutions.

Compared in Fig. 4 are the amide protons (H_Ns) and the α protons (H_αs) of the ^1H NMR spectra of compounds **1** and **2**[20] (Figs. 4a and 4b). The chemical shift correspondence observed in these fingerprint regions of Cys^1–Pro–Leu–Cys^4 of **1** and **2** allows us to estimate that these two compounds possess a common Cys^1–Pro–Leu–Cys^4 structure. The fact that the two compounds also exhibited similar NOESY patterns[44,45] with respect to the Cys^1–Pro–Leu–Cys^4 moiety has evidenced the reliability of this estimation. Based on these, the pro-chiralities (R and S) of $Cys^{1,4}$ $H_\beta^{(1,2)}$ and Pro $H_{\beta,\delta}^{(1,2)}$ of compound **1** were estimated to be the same as those of compound **2**, where the superscripts in parentheses 1 and 2 on $H_{\beta,\delta}$ mean the numberings of the ^1H NMR spectral

Table 1. Result of EXAFS Analysis[a)]

No.	Parameter	N	r / Å	ΔE / eV	$\Delta C^{b)}$ / $(\sigma)^{c)}$	R/%
1	HgS_2[d)]	2.07	2.326	0	−0.000705	0.08285[g)]
2	HgS_3[e)]	2.19	2.329	0	−0.001319	0.04815[g)]
3	HgS_4[f)]	2.00	2.344	0	−0.004725	0.1521[g)]
4	HgS_2[d)]	2.13	2.329	0	−0.000462	0.4164[h)] 0.0626[i)]
5	HgS_3[e)]	2.16	2.323	0	−0.001369	0.1391[h)] 0.0371[i)]
6	HgS_4[f)]	1.96	2.316	0	−0.005040	0.2155[h)] 0.0180[i)]
7	Theor[j)]	2.0	2.330	7.0	0.061[c)]	

a) FT k range: 3.2—14.2 $Å^{-1}$. Back FT R range = 1.40—2.50 Å. CF k range = 4.0—13.65 $Å^{-1}$. b) $\sigma^2_{obs}-\sigma^2_{mdl}$: σ_{obs} = Debye–Waller-like factor for compound **1**. σ_{mdl} = Debye–Waller-like factors for model compounds. We inputted σ = 0.00 Å for the model systems. c) Debye–Waller-like factor obtained from FEFF simulation.[35)] d) Backscattering amplitude and phase shift parameters were extracted from the analysis of $[Hg(SCH_3)_2]$. e) Backscattering amplitude and phase shift parameters were extracted from the analysis of $(NEt_4)[Hg(S\text{-}t\text{-}C_4H_9)_3]$ f) Back scattering amplitude and phase shift parameters were extracted from the analysis of $(NEt_4)_2[Hg(SC_4H_4Cl)_4]$. g) Curve fitting: refined by $R=\Sigma\{k^3\chi_{obs}-k^3\chi_{calc}\}^2/\Sigma\{k^3\chi_{obs}\}^2$. h) Ratio method: refinement parameter for amplitude. i) Ratio method: refinement parameter for phase. j) FEFF 6.01[35)] was used for $Hg(SC)_2$ core: Hg–S = 2.33 Å, S–C = 1.728 Å, ∠Hg–S–C = 110.63°. The best simulation was obtained at the Debye temperature (Θ_D) = 575 K, simulation temperature = 298 K, core hole reduction factor (SO^2) = 0.85, and number of scattering paths (nleg) = 8. Multiple scattering paths at> 4.66 Å were neglected.

Table 2. Result of Multiple Scattering Calculation for $Hg(SC)_2$,[a)] the Core of [(Boc–CPLCGA–OMe)Hg], by FEFF 6.01[b,c)]

No.	σ^2	Amp ratio	D_{eg}	N_{legs}	R_{eff}/Å
1	.00367	100.00	2.00	2	2.3300
2	.01130	26.09	2.00	2	3.3548
3	.01013	23.41	4.00	3	3.7066
4	.01118	7.23	2.00	4	4.0584
5	.00731	6.64	2.00	3	4.6600
6	.00731	17.50	2.00	4	4.6600

a) See Fig. 2. b) FEFF 6.01[35)] by Rehr and co-workers. c) For the conditions of FEFF calculation, see Table 1.

bands from high- to low field. The final determination of the pro-chiral assignments for Pro $H^{(1,2)}_{\delta}$ was made by comparing the off-diagonal peak intensities between Pro $H^{(1,2)}_{\delta}$ and Pro $H^{(1,2)}_{\beta}$ in the NOESY and ROESY spectra. On the other hand, the final pro-chiral assignments for $Cys^{1,4}$ $H^{(1,2)}_{\beta}$ and Pro $H^{(1,2)}_{\beta}$ were determined by a comparison of the results of MD (without constraint) and RMD, as is shown later. Proline was determined to be *trans* from the ^{13}C chemical shifts of Pro C_{β} (30.26 ppm) and Pro C_{γ} (24.64 ppm).[46)]

In order to estimate hydrogen bonded H_Ns, we observed the temperature dependence of the chemical shifts over the range 240—300 K. All of the amide protons possessed good linearities in the temperature range 270—300 K; however, below 260 K, they showed broadening. The slopes of the temperature-dependent chemical shifts for the H_Ns (δ/T; ppm/deg) of compounds **1** and **2** in DMF-d_7 and DMSO-d_6 are summarized in Table 3. δ/T indicates the degree of the masking of the hydrogen-bonded H_N from the solvent;[46)] however, the values are relative, and seem to be dependent on the species. Detailed studies for the δ/T of the H_Ns of the compounds involving cystens were performed by Balaram and his co-workers using NOE.[47)] Referring to their results concerning the disulfide forms of Cys–Pro–X–Cys,[47b,47c)] we estimated from our result for compound **1** (Table 3) that Leu H_N and Cys^4 H_N of compound **1** in DMF-d_7 are hydrogen bonded and effectively masked from the access of the solvent molecules, whereas Cys^1 H_N and Ala H_N are exposed to the solvent. Gly H_N situates at the intermediate of these two cases. The same tendency is recognized for the δ/T values in DMSO-d_6. The effect of the alteration of the solvents seems to be parallel for the Cys^1 H_N, Leu H_N, and Cys^4 H_N of compound **2**, except for the Cys^4 H_N in DMF-d_7, the δ/T value of which indicates the exposure of the H_N in DMF-d_7.

The ^1H-^1H atom distances were extracted from the off-diagonal peak intensities of the PS NOESY and ROESY signals, in which the DMF-d_7 solution gave positive NOEs, whereas the DMSO-d_6 solution gave negative ones. The

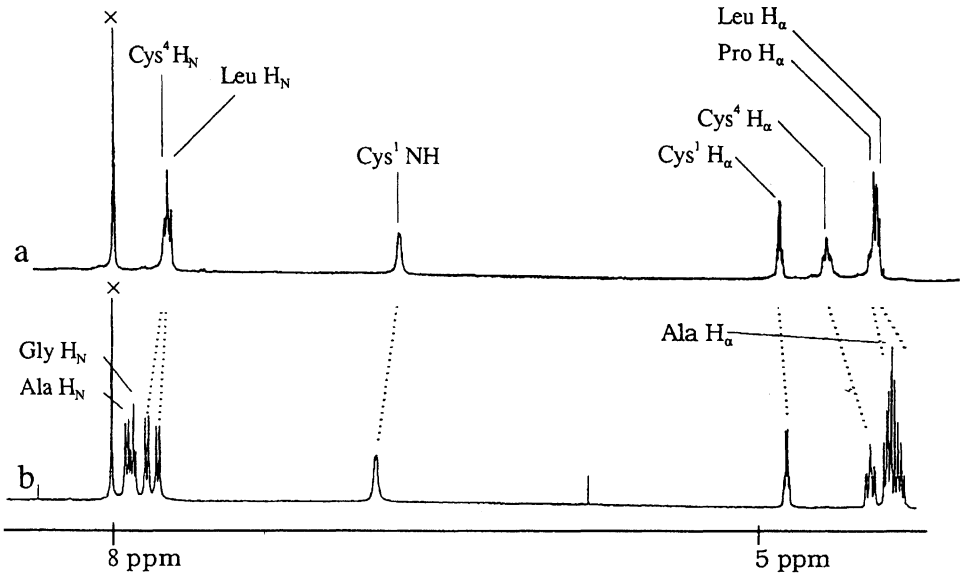

Fig. 4. The ^{1}H NMR fingerprint regions of compounds **1** nad **2** observed at 25 °C, 500 MHz, DMF-d_7. (a) Compound **2**. (b) Compound **1**.

Table 3. Temperature Dependence[a] of the Chemical Shift[b] of Amide Protons of Compounds **1** and **2** in DMF-d_7 and DMSO-d_6

Compound	Cys^{1}H$_N$	Leu H$_N$	Cys^{4}H$_N$	Gly H$_N$	Ala H$_N$	Solution	Temp range/K
1	0.00779	0.00503	0.00504	0.00632	0.00834	DMF-d_7	260—300 K
1	0.00618	0.00225	0.00318	0.00491	0.00566	DMSO-d_6	292—316 K
2	0.0082	0.0041	0.0077	—	—	DMF-d_7	223—298 K
2	0.0055	0.0021	0.0030	—	—	DMSO-d_6	298—318 K

a) Observed at 270—300 K. b) δ/T; ppm·deg^{-1}.

geminal Pro H$_\beta$ intensity was used as the internal standard (d_{H-H} = 1.752 Å) for the distance estimation. The atomic distances, including the distal protons of side chains (Pro H$_\delta$, Leu H$_{\gamma,\delta}$), were ignored because of differences in the relaxation time. On the basis of this estimation, the lower and upper limits of each ^{1}H–^{1}H distance were determined according to the classification described in a previous paper.[20] Listed in Table 4 are the distances, including those for the S–Hg–S bridge, as well as those for the Hg center obtained from XAFS experiments.

Structural Analysis

Molecular-dynamics (MD and RMD) calculations were carried out using AMBER ver. 3.0 revision A.[23] A distance geometry (DG) calculation was performed with the program CADMOS described previously.[20,25] Molecular graphics images were produced using the MidasPlus software system ver. 1.5.[48] All of the data were processed on HP 9000/735 and Iris 4D 25G workstations.

MD and RMD. Because of the similarity of the Hg(Cys–S)$_2$ cores in compounds **1** and **2**, as shown by XAFS experiments, we used for compound **1** the same MD parameters which we previously determined for compound **2**.[20] Prior to each series of MD (RMD) calculation, molecular mechanics energy minimizations were carried out for 200 randomly generated conformations, from which 20 structures with the lowest energies were selected as the starting points of MD and RMD calculations. MD (RMD) calculations were then performed under vacuum conditions with a step time of 1 fs, employing SHAKE,[49] where a distance-dependent dielectric constant, $\varepsilon_{ij} = r_{ij}$, was used. The temperature was decreased stepwise from 1000 K (0—10 ps) to 700 K (10—20 ps), 450 K (20—30 ps), and finally to 300 K (30—80 ps), with a time constant of 0.1 ps for heat-bath coupling. In the RMD calculation, the constraint given in Table 4 was processed by using a subroutine involving Nilges's quadratic potential.[20,24] The structures averaged for the final 10 ps were used for a comparison.

The ^{1}H NMR numbering of the H$_\beta^{(1,2)}$ protons of cysteines, 1 and 2, does not correspond to the numbering of Cys H$_\beta^{(1,2)}$ in the AMBER parameter file. Hence, in order to determine the absolute assignment of these protons, we performed MD and RMD calculations independently, where the RMD calculation was performed for 4 different types of combinations of Cys^1 H$_\beta^{(1,2)}$ and Cys^4 H$_\beta^{(1,2)}$ in the constraint table, in which the numbering of the H$_\beta$ protons obeys AMBER. From a comparison of the potential energies and molecular shapes obtained from these four series RMD calculations with those

Table 4. Distance Constraint for Compound **1**[a)]

Atom 1	Atom 2	Distance constraint/Å		Violation[b)]
		LL[c)]	UL[d)]	
Hg	Cys^4 S	2.328	2.332[e)]	−0.082
Hg	Cys^4 C_β	3.314	3.316[f)]	−0.160
Cys^1S	Cys^4 S	4.658	4.662[e)]	−0.162
Cys^1H_N	Cys^1H_α	2.30	2.70	0.016
Cys^1H_N	$Cys^1H_\beta^{(1),\ pro\text{-}R}$	2.40	3.50	0.000
Leu H_N	Leu H_α	2.30	2.70	0.097
Leu H_N	Pro H_α	2.40	3.50	0.000
Leu H_N	Leu $H_\beta^{(1)}$	1.90	4.00	0.000
Cys^4H_N	Cys^4H_α	2.50	2.93	0.000
Cys^4H_N	$Cys^4H_\beta^{(1),\ pro\text{-}R}$	0.00	2.60	0.000
Cys^4H_N	Pro H_α	2.80	4.20	0.000
Cys^4H_N	Leu H_α	2.00	3.00	0.000
Gly H_N	Gly $H_\alpha^{(1)}$	2.19	2.50	0.000
Gly H_N	Cys^4H_α	0.00	2.60	0.000
Gly H_N	$Cys^4H_\beta^{(1),\ pro\text{-}R}$	3.20	5.00	0.000
Ala H_N	Ala H_α	2.19	2.50	0.000
Ala H_N	Ala $H_\beta^{(1)}$	2.30	4.70	0.000
Cys^1H_α	$Cys^1H_\beta^{(1),\ pro\text{-}R}$	2.23	2.60	0.000
Cys^1H_α	$Cys^1H_\beta^{(2),\ pro\text{-}S}$	2.40	2.80	−0.275
Cys^1H_α	Pro $H_\delta^{(1)}$	0.00	2.60	0.000
Cys^1H_α	Pro $H_\delta^{(2)}$	0.00	2.60	0.032
Pro H_α	Pro $H_\beta^{(1)}$	2.23	2.60	−0.072
Pro H_α	Pro $H_\beta^{(2)}$	2.23	2.60	0.026
Pro H_α	Pro $H_\delta^{(1)}$	2.80	4.20	0.000
Pro H_α	Pro $H_\delta^{(2)}$	3.20	5.00	0.000
Cys^4H_α	$Cys^4H_\beta^{(1),\ pro\text{-}S}$	2.60	3.04	0.000
Cys^4H_α	$Cys^4H_\beta^{(2),\ pro\text{-}R}$	2.23	2.60	0.000
Pro $H_\beta^{(1)}$	Pro $H_\delta^{(1)}$	2.40	3.50	0.000
Pro $H_\beta^{(2)}$	Pro $H_\delta^{(2)}$	2.80	4.20	0.000
$Cys^1H_\beta^{(2),\ pro\text{-}S}$	Pro $H_\delta^{(1)}$	2.40	3.50	0.000
$Cys^1H_\beta^{(2),\ pro\text{-}S}$	Pro $H_\delta^{(2)}$	0.00	2.60	0.000

a) Superscripts 1 and 2 on $H_{\beta,\delta}$ protons of $Cys^{1,4}$ and Pro denote numbering of the ^{1}H NMR bands from the hight field to the lowfield. b) The violations are for the lowest constraint structure obtained from the RMD calculation assuming Cys^1 S–Leu H_N. + and − denote violations from the upper and lower limits, respectively. c) Lower Limit. d) Upper Limit. e) Determined by EXAFS analysis. f) ∠Hg–S–Leu H_N = 95—110° and ∠Cys^1 C_β–S–Leu H_N = 95—110° were assumed to calculate this value, referring to the bond angle value ∠Lp–S–H = 96.7° in AMBER ver 3.0 revision A.[23)]

of the MD calculations, which are free from a distance constraint, the correspondence between the NMR numbering and the AMBER numbering was determined. The pro-chiralities, R and S, of the cysteines were then determined by computer graphics from the lowest energy structures of the RMD calculations. The results are given in Table 4.

In the MD calculation at the first stage we obtained the 12 lowest enegy structures, which converged to those having the same conformations in the three N-terminal residues. These were classified into two types of structures: type A and type B. For type A structure, the rmsd of the C, N, and S atoms of the Cys^1–Pro–Leu–Cys^4 main chain loop and that for Cys^1 C_β, C_α, C(O), Pro N, C_α, C(O), and Leu N seven atoms were < 0.865 Å and < 0.27 Å, respectively. Those for type B (this ensemble involved the lowest energy structure) were 0.600 Å and 0.14 Å. As can be seen in Fig. 5a (type A) and Fig. 5b (type B), both have the same hydrogen bond, Cys^1 S–Leu H_N, which is also common to compound **2**. The structures exhibit the following additional hydrogen bonds: Pro CO–Cys^4 H_N for type A; Pro CO–Cys^4 H_N and Cys^1 CO–Gly H_N for type B.

Among the four series of RMD calculations carried out at the second stage, the combination which afforded type A structres gave the lowest energies. Although this series of calculations also afforded type B structures, they showed slightly larger violations than those of type A structures for the distance constraint. The 9 structures which converged at type A are shown in Fig. 5c superimposed at the C, N,

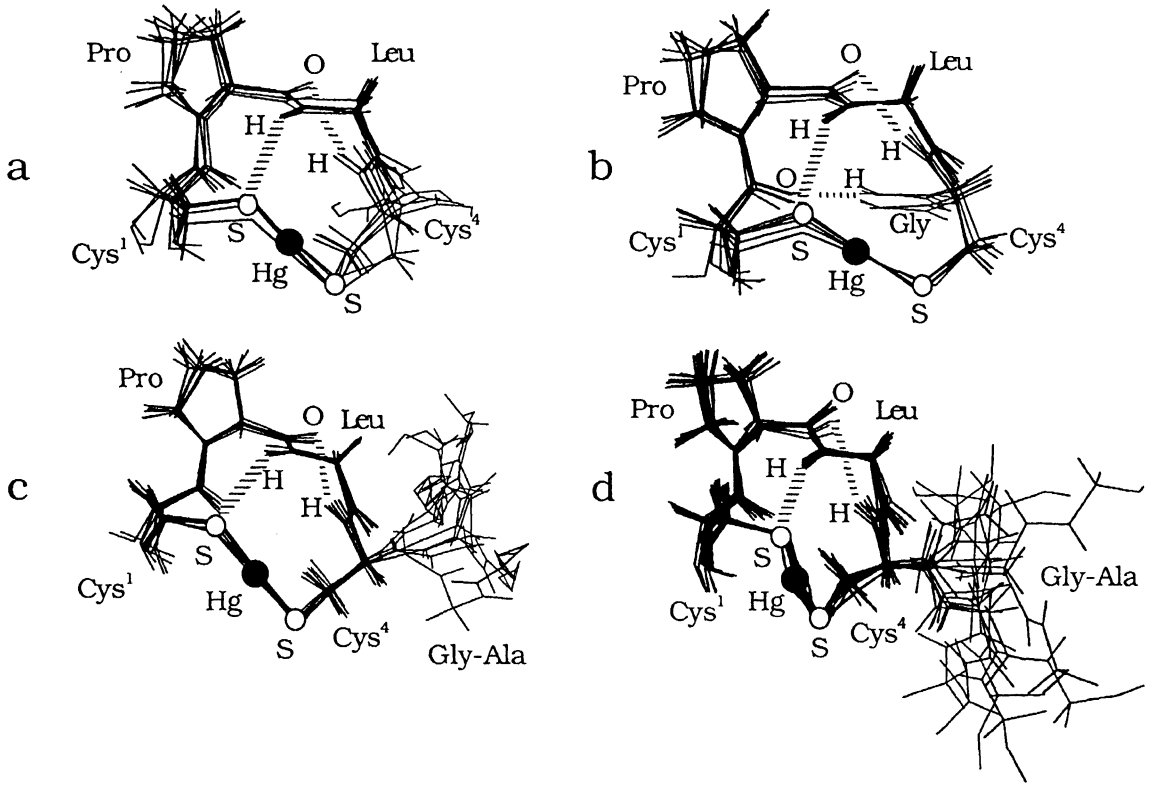

Fig. 5. Converged structures of [(Boc–Cys^1–Pro–Leu– Cys^4–Gly–Ala–OMe)Hg], **1**. ○ and ● in the figures depict S and Hg, respectively. (a) Six structures belonging type A from the MD calculation, superimposed at the C, N, and S atoms of Cys–Pro–Leu–Cys main chain loop. rmsd < 0.865 Å. The dashed lines show the Leu H_N– Cys^1 S and Pro CO–Cys^4 H_N hydrogen bonds. (b) Six structures belonging type B from the MD calculation, superimposed at the atoms as in (a). The dashed lines show the Leu H_N-Cys^1 S, Pro CO–Cys^4 H_N, and Cys^1 CO–Gly H_N hydrogen bonds. rmsd < 0.6 Å. (c) Nine converged structures obtained from the RMD calculation, superimposed at the same atoms as in (a). rmsd < 0.32 Å. (d) Twelve converged structures obtained from the DG calculation, superimposed at the same stoms as in (a). rmsd < 0.842 Å.

and S atoms of the Cys^1–Pro–Leu–Cys^4 main-chain loop (rmsd < 0.32 Å). The rmsd for the N-terminal 7 atoms (Cys^1 C_β, C_α, C(O), Pro N, C_α, C(O), and Leu N) was 0.090 Å.

DG. A DG calculation was performed independently of the MD and RMD calculations mentioned above, because of its advantage to give experimentally the most possible structures, although it lacks information concerning the potential energy. Four series of DG calculations, were carried out corresponding to the four types of constraints used in RMD. In this calculation. we assumed the existence of the Cys^1 S–Leu H_N hydrogen bond with reference to the results of MD and RMD calculations mentioned above, as well as to the XAFS and NMR similarlities of the Cys^1–Pro–Leu–Cys^4/Hg moieties between compounds **1** and **2**. Each of the four series of DG calculations was carried out for 150 structures, which were generated randomly. The results were compared in the form of histograms of the target functions,[25] as well as the molecular shapes. Also, in this calculation the combination that achieved the lowest target functions gave structures compatible with type A from the MD calculation. The 12 structures obtained from these calculations are shown in Fig. 5d, in which they are superimposed at the C, N, and S atoms of the main chain loop (rmsd < 0.842 Å). The rmsd for the N-terminal 7 atoms (Cys^1 C_β, C_α, C(O), Pro N, C_α, C(O), and Leu N) was 0.112 Å.

Consequently, it is concluded that compound **1** takes the type A structure in DMF (Figs. 5a, 5c, and 5d).

Discussion

New Turn. The linear coordinate Hg^{2+} in compound **1** allows for the formation of two hydrogen bonds, Cys^1 S–Leu H_N and Pro CO–Cys^4 H_N (Fig. 1b). The molecular parameters for the second hydrogen bond in the structure, which achieved the lowest violation in the RMD calculation, are r(O–H)=2.15 Å, r(O–N)=2.91 Å, and ∠(O–H–N)=143.5°. This bonding scheme for compound **1** is the same as that observed for compound **2**, but differs from those observed in biological systems, Cys^i–X–Y–Cys^{i+3}/M^{2+}, which are dominated by tetrahedral metal ions, Fe^{2+} and Zn^{2+}, and involve two hydrogen bonds, Cys^i–S–Y^{i+2} H_N and Cys^i–S–Cys^{i+3} H_N (Fig. 1a).[5,7–12] The former hydrogen bond in compound **1**, Cys^1 S–Leu H_N, is common to that observed in the metalloenzymes. The latter bond, Pro CO–Cys^4 H_N, is the same kind as those observed in the γ-type turns of proteins.[50] the peptide folding observed for the Pro–Leu–Cys^4 of compound **1** is close to that observed for the mirror-image γ-type turn. In practice, ϕ and ψ of Leu in the 9 RMD structures of Fig. 5c are distributed in the range of $\phi = -85°$ to $-74°$ and

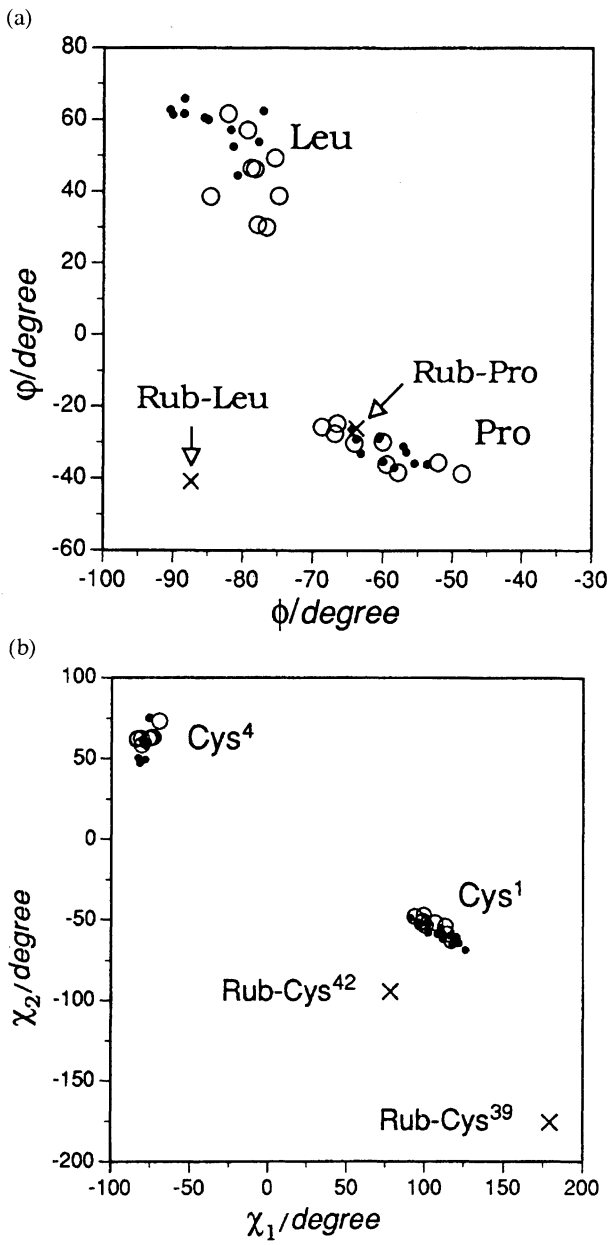

Fig. 6. (a top) Ramachandran plot showing the deviations of the Pro and Leu (ϕ, ψ) for the 9 converged structures from the RMD (●) calculation of compound **1**. The corresponding (ϕ, ψ) sets for compound **2** (○), reported in our previous paper,[20] and the rubredoxin core (×). (b, bottom) Plots of the C_α– C_β torsion angles (χ_1, χ_2) for Cys^1 and Cys^4 of compound **1**, where χ_1 and χ_2 are defined as $\angle N\text{–}C_\alpha\text{–}C_\beta\text{–}S$ and $\angle C_\alpha\text{–}C_\beta\text{–}S\text{–}Hg$, respectively.

$\psi = +30°$ to $+62°$ (see Fig. 6a), whereas those of γ-type turn are in the range of $\phi = +70°$ to $85°$ and $\psi = -60°$ to $-70°$).[51] The slight deviation from the ideal mirror image is probably caused by the coexistence of Cys^1 S–Leu H_N. Consequently, it is possible to confirm that compound **1** represents a new type of turn structure which is the hybrid of ordinary types: Cys^i–X–Y–Cys^{i+3}/M^{2+} and mirror-image γ turn.

As can be seen from Fig. 5c, the RMD calculation indicates that the Gly–Ala residues in compound **1** is directed oppositely to the main chain loop Cys–Pro–Leu–Cys/Hg^{2+}; therefore, the hydrogen bond, Pro CO–Cys^4 H_N, seems to be exposed to solvents as in the case of compound **2**. However, an MD calculation has clarified that the Gly–Ala part moves flexibly as if it covers the hydrogen bond from the access of the solvents (see Fig. 5a). This is what we expected, and the reason why we observed a low δ/T for the Cys^4 H_N in compound **1**, which leads to the hydrogen bonding character of the H_N, but not in compound **2**.

Conformation Control by Metal Ion in Cys–Pro–Leu–Cys/Hg(II). The agreement of the XAFS of compound **1** with that of compound **2** indicates that the $Hg(Cys\text{–}S)_2$ units of both compounds take almost the same structure. This structural agreement is expanded to the peptide parts surrounding the inorganic centers. Figure 6a exhibits Ramachandran plots[51] for the Pro and Leu residues of the 9 RMD structures, which converged at type A, with those of compound **2**. The (ϕ, ψ) plots of Cys^4 and Gly residues were not shown here because of their large deviation, especially in ψ (see Fig. 5c). As can be seen from Fig. 6a, although the areas of Pro and Leu (ϕ, ψ)s of compounds **1** and **2** overlap well with each other, the Leu (ϕ, ψ)s of these compounds differ from those of Cys^i–X–Y–Cys^{i+3} in proteins, as manifested in the figure by that for *D. vulgaris* rubredoxin.[7] On the other hand, Fig. 6b depicts the rotations of $Cys^{1,4}$, (χ_1, χ_2), with respect to the Cys S–Hg bonds, where χ_1 and χ_2 are defined as $\angle N\text{–}C_\alpha\text{–}C_\beta\text{–}S$ and $\angle C_\alpha\text{–}C_\beta\text{–}S\text{–}Hg$, respectively. This figure indicates that the rotations around $Cys^{1,4}$ for compounds **1** and **2** are the same, but are different when compared to those of the rubredoxin. It should be pointed out, however, that our computer experiment afforded no diffrence in the conformational energy between the Cys^i–X–Y–Cys^{i+3} sequences of these two cases: linear coodinnate Hg^{2+} and $Fe^{2+}(Zn^{2+})$.[52]

Our conformational analyses on compound **1** showed no additional hydrogen bonds between the Cys–Pro–Leu–Cys core and Gly–Ala part, as observed in the rubredoxin core (Fig. 1c→Fig. 1a). The residue extension from Cys^1–Pro–Leu–Cys^4 to Cys^1–Pro–Leu–Cys^4–Gly–Ala also brought about no dihedral angle change in the Cys^1–Pro–Leu–Cys^4 part (Fig. 1d→Fig. 1b). In other words, the conformation of the tetrapeptide is unaffected by any intramolecular interactions attributable to the addition of Gly–Ala residues. This structural independence of the Cys^1–Pro–Leu–Cys^4/Hg^{2+} part in compound **1** would be because Gly–Ala is directed opposite to the main chain loop (Fig. 5c). The Hg^{2+} controls the proximal rotations (χ_1,χ_2) of $Cys^{1,4}$ and thereby affects the distal rotations (ϕ, ψ) of Pro and Leu, and the directions of the N- and C-termini of the cysteines. In contrast to these model compounds, the tetrahedral ions in proteins control the directions of both the N- and C-termini of the Cys^is and Cys^{i+3}s (Figs. 1a and 1c) of the Cys^i–X–Y–Cys^{i+3} moieties, which probably allows for the additional multiple hydrogen bondings between the tetrapeptide units and the following A–B residues, and extremely stabilizes the conformation energies of the Cys^i–X–Y–Cys^{i+3}–A–B/M^{2+} cores.

Consequently, it may be possible to propose that the Cys^1–X–Y–Cys^4 conformations are dominated by the coordination geometries of the central metal ions.

We thank Professor J. J. Rehr for the license agreement of the FEFF 6.01 program. This work was supported by a Grant-in-Aid for Scientific Research No. 04225231 from the Ministry of Education, Science and Culture.

References

1) J. S. Richardson and D. C. Richardson, "Prediction of Protein Structure and the Principles of Protein Conformation," ed by G. D. Fasman, Plenum, New York (1989).

2) a) C. D. Stout, "Iron Sulfur Proteins," ed by T. G. Spiro, Wiley-Interscience, New York (1982), Vol. 4, Chap. 3, p. 97; b) H. Matsubara and K. Saeki, "Iron Sulfur Proteins," ed by R. Cammack, Academic, San Diego (1992), p. 223.

3) B. L. Vallee and D. S. Auld, *Proc. Natl. Acad. Sci. U.S.A.*, **87**, 22 (1990); "Zinc Enzymes," ed by T. G. Spiro, Wiley-Interscience, New York (1983), Vol. 5.

4) a) J. M. Berg, *Annu. Rev. Biophys. Biophy. Chem.*, **19**, 405 (1990); b) J. M. Berg, *Acc. Chem. Res.*, **28**, 14 (1995).

5) M. Vasåk and J. H. R. Kägi, "Metal Ions in Biological Systems," ed by H. Siegel, Marcel-Dekker, New York (1983), Vol. 15, p. 213.

6) a) T. V. O'Halloran, *Science*, **261**, 715 (1993); b) R. J. P. Williams, *Biochem. Soc. Trans.*, **18**, 689 (1990).

7) a) K. D. Watenpaugh, L. C. Sieker, and L. H. Jensen, *J. Mol. Biol.*, **131**, 509 (1979); b) M. Frey, L. C. Sieker, F. Payan, R. Haser, M. Bruschi, G. Pepe, and J. LeGall, *J. Mol. Biol.*, **197**, 525 (1987); c) E. T. Adman, L. C. Sieker, and L. H. Jensen, *J. Mol. Biol.*, **217**, 337 (1991).

8) W. F. Furey, A. H. Robbins, L. L. Clancy, D. R Winge, B. C. Wang, and C. D. Stout, *Science*, **231**, 704 (1986).

9) H. Eklund, B. Nordstrom, E. Zeppenzauer, G. Soderlund, I. Ohlsson, T. Borwe, B-O. Soderberg, O. Tapia, C-I. Branden, and A. Akeson, *J. Mol. Biol.*, **102**, 27 (1976); H. Li, W. A. Hallows, J. S. Punzi, V. E. Marquez, H. L. Carrell, K. W. Pankiewicz, K. A. Watanabe, and B. M. Goldstein, *Biochem.*, **33**, 23 (1994).

10) a) B. F. Luisi, W. X. Xu, Z. Otwinowski, L. P. Freedman, K. R. Yamamoto, and P. B. Sigler, *Nature*, **352**, 497 (1991); G. Zhang, M. G. Kazanietz, P. M. Blumberg, and J. H. Hurley, *Cell*, **81**, 917 (1995); b) N. P. Pavletch and C. O. Pabo, *Science*, **252**, 809 (1991); c) L. Fairall, J. W. R. Schwabe, L. Chapman, J. T. Finch, and D. Rhodes, *Nature*, **366**, 483 (1993); d) P. J. Krauris, A. R. C. Rain, P. L. Gadhavi, and E. D. Laue, *Nature*, **356**, 448 (1992); e) J. D. Baleja, R. Marmolstein, S. C. Harrison, and G. Wagner, *Nature*, **356**, 450 (1992); R. Marmorstein, M. Carey, M. Ptashne, and S. C. Harrison, *Nature*, **356**, 408 (1992).

11) H. M. Ke. W. N. Lipscomb, Y-J. Cho, and R. B. Honzatko, *J. Mol. Biol.*, **204**, 725 (1988); J. E. Gouaux, R. C. Stevens, and W. N. Lipscomb, *Biochemistry*, **29**, 7702 (1990).

12) a) E. T. Adman, L. C. Sieker, and L. H. Jensen, *J. Biol. Chem.*, **251**, 3806 (1976); b) C. D. Stout, *J. Mol. Biol.*, **205**, 545 (1989).

13) K. Furuyama, H. Matsubara, T. Tsukihara, and Y. Katsube, *J. Mol. Biol.*, **210**, 383 (1989).

14) a) C. W. Carter, Jr., J. Kraut, S. T. Freer, N. Xuong, and R. A. Alden, *J. Biol. Chem.*, **249**, 6339 (1974); b) E. Adman, K. D. Watenpaugh, and L. H. Jensen, *Proc. Natl. Acad. Sci. U.S.A.*, **72**, 4854 (1975).

15) C. R. Kissinger, C. Sieiker, E. T. Adman, and L. H. Jensen, *J. Mol. Biol.*, **219**, 693 (1991).

16) T. Tsukihara, K. Fukuyama, M. Nakamura, M. Mizushima, T. Harioka, M. Kusunoki, Y. Katsube, T. Hase, and H. Matsubara, *J. Mol. Biol.*, **216**, 399 (1990).

17) A. H. Robbins and C. D. Stout, *Proc. Natl. Acad. Sci. U.S.A.*, **86**, 3639 (1989).

18) a) T. Takano and R. E. Dickerson, *J. Mol. Biol.*, **153**, 95 (1981); b) G. W. Bushnell, G. V. Louie, and G. D. Brayer, *J. Mol. Biol.*, **214**, 585 (1990); c) C. Frazao, J. Morais, P. M. Matias, and M. A. Carrendo, *Acta Crystallogr., Sect. D*, **50**, 233 (1994).

19) a) S. K. Katti, D. M. LeMaster, and H. Eklund, *J. Mol. Biol.*, **212**, 167 (1990); b) P. Sodano, T-h. Xia, J. H. Bushweller, O. Björnberg, A. Holmgren, M. Billeter, and L. Wurtlich, *J. Mol. Biol.*, **221**, 1311 (1991); c) P. Sodano, K. V. R. Chary, O. Björnberg, A. Holmgren, B. Kren, and J. A. Fuchs, *Eur. J. Biochem.*, **200**, 369 (1991).

20) T. Yamamura, T. Watanabe, A. Kikuchi, M. Ushiyama, T. Kobayashi, and H. Hirota, *J. Phys. Chem.*, **99**, 5525 (1995).

21) B. K. Teo, "EXAFS: Principles and Data Analysis," Springer-Verlag, Berlin (1986).

22) J. Jeener, B. H. Meier, P. Bauchmann, and R. R. Ernst, *J. Chem. Phys.*, **71**, 4546 (1979).

23) "AMBER Revision A," S. J. Weiner, P. A. Kollman, D. T. Nguyen, and D. A. Case, *J. Comput. Chem.*, **7**, 230 (1986).

24) a) G. M. Clore, A. M. Gronenborn, A. T. Brünger, and M. Karplus, *J. Mol. Biol.*, **186**, 435 (1985); b) M. Nilges, A. M. Gronenborn, A. T. Brünger, and G. M. Clore, *Protein Eng.*, **2**, 27 (1988).

25) W. Braun and N. Go, *J. Mol. Biol.*, **186**, 611 (1985).

26) W. Walter, M. Stephen, and K. Heyns, *Chem. Ber.*, **99**, 3213 (1966); D. F. Veber, J. D. Milkowski, S. L. Varga, R. G. Denkewalter, and R. Hirschman, *J. Am. Chem. Soc.*, **94**, 5456 (1972).

27) Boc–Cys(Acm)–Pro–Leu–Cys(Acm)–Gly–Ala–OMe, **3**. Yield 62.9% (purity: 99.5% by HPLC). ^{1}H NMR (25 °C, 500 MHz, DMSO-d_6) δ = 0.847 (6H, d of d, Leu H_δ), 1.281 (3H, d, Ala H_β), 1.369 (9H, s, Boc–CH_3), 1.463 (2H, m, Leu H_β), 1.606 (1H, m, Leu H_δ), 1.838 (3H, d, Acm–CH_3), 1.81—1.99 (2H, m, Pro H_γ), 1.81—2.11 (2H, m, Pro H_γ), 2.59—2.96 (4H, $Cys^{1,4}$ H_β), 3.616 (5H, Pro H_δ + Ala–OMe), 3.822 (2H, d, Gly H_α), 4.16—4.53 (7H, $Acm^{1,4}$–CH_2, Leu H_α, $Cys^{1,4}$ H_α, Pro H_α), 7.120 (1H, d, Cys^1 H_N), 7.898 (1H, d, Ala H_N), 7.998 (1H, d, Cys^4 H_N), 8.11—8.26 (2H, Leu H_N + Gly H_N), 8.514 (2H, $Acm^{1,4}$ H_N). Anal. Found: C, 48.77; H, 7.03; N, 13.74%. Calcd for $C_{34}H_{58}N_8O_{11}S_2 \cdot 0.5H_2O$: C, 49.05; H, 7.20; N, 13.46%. Mass Spectrum (m^+/z) = 841 (theor. for **3**·Na) = 841.

28) N. Ueyama, M. Nakata, and A. Nakamura, *Bull. Chem. Soc. Jpn.*, **58**, 464 (1985).

29) Anal. Found: C, 36.25; H, 5.23; N, 9.11%, Na, trace; Cl, Beilstein, negative. Calcd for $C_{28}H_{46}N_6O_9S_2Hg \cdot 3H_2O$: C, 36.18; H, 4.99; N, 9.04; Na 0.0; Cl 0.0%. Mass spectrum (m^+/z) = 899 (theor. for **1**·Na with ^{202}Hg = 899). The isomer pattern of the parent peak agreed with that of the theoretical. ^{1}H NMR (25 °C, 500 MHz, DMF-d_7) δ = 0.851—0.915 (6H, d of d, Leu $H_{\delta 1,2}$), 1.331—1.345 (3H, d, Ala H_β), 1.416 (9H, s, Boc–CH_3), 1.657—1.672 (2H, m, Leu H_β), 1.73 (1H, m, Leu H_χ), 1.95—2.05 (1H, m, Pro H^1_β), 2.00—2.10 (2H, m, Pro H_γ), 2.31—2.37 (1H, m, Pro H^2_β), 3.26—3.32 (1H, q, Cys^4 H^1_β), 3.45, 3.51 (1H, d of d, Cys^1 H^1_β), 3.45, 3.48 (1H, d of d, Cys^4 H^2_β), 3.65—3.70 (1H, Cys^1 H^2_β), 3.667 (3H, s,

Ala–OMe), 3.80—3.93 (1H, q of d, Gly H_α), 3.82—3.90 (1H, m, Pro $H_{\delta 1}$), 3.92—4.00 (1H, m, Pro $H_{\delta 2}$), 4.32—4.43 (3H, m, Leu H_α, Pro H_α, Ala H_α), 4.45—4.52 (1H, t of d, Cys^4H_α), 4.869—4.879 (1H, q, Cys^1 H_α), 6.780, 6.789 (1H, d, Cys^4 H_N, 7.792, 7.810 (1H, d, Cys^4 H_N), 7.845, 7.861 (1H, d, Leu H_N), 7.905, 7.917, 7.929 (1H, t, Gly H_N), 7.940, 7.954 (1H, d, Leu H_N).

30) 2.5 GeV, 280—380 mA.

31) N. Kosugi and H. Kuroda, "EXAFS 2, SRI Report," **1985**; No. 2. T. Yokoyama, H. Hamamatsu, and T. Ohta,"Program EXAFSH Version 2.1," The University of Tokyo, 1994.

32) J. A. Victoreen, *J. Appl. Phys.*, **19**, 855 (1948).

33) E. A. Stern, D. E. Sayers, and F. W. Lytle, *Phys. Rev.*, **B11**, 4836 (1975).

34) D. E. Sayers, E. A. Stern, and F. W. Lytle, *Phys. Rev. Lett.*, **27**, 1204 (1971).

35) a) J. J. Rehr and R. C. Albers, *Phys. Rev.*, **B41**, 8139 (1990); b) J. J. Rehr, S. I. Zabinski, and R. C. Albers, *Phys. Rev. Lett.*, **69**, 3397 (1992).

36) A. Bax and M. F. Summers, *J. Am. Chem. Soc.*, **108**, 2093 (1986).

37) a) A. A. Bothner-By, R. L. Stephens, J. Lee, C. D. Warren, and R. W. Jeanloz, *J. Am. Chem. Soc.*, **106**, 811 (1984); b) A. Bax and D. G. Davis, *J. Magn. Reson.*, **63**, 207 (1985); c) H. Kessler, C. Griesinger, R. Kerssebaum, K. Wagner, and R. R. Ernst, *J. Am. Chem. Soc.*, **109**, 607 (1987).

38) D. Marion and K. Würtrich, *J. Magn. Reson. Commun.*, **113**, 967 (1983).

39) D. C. Bradley and N. R. Kuncher, *J. Chem. Phys.*, **40**, 2258 (1964).

40) S. P. Watton, J. G. Wright, F. M. MacDonnell, J. W. Bryson, M. Sabat, and T. O'Halloran, *J. Am. Chem. Soc.*, **112**, 2824 (1990).

41) S. Choudhury, I. G. Dance, P. J. Guerney, and A. D. Rae, *Inorg. Chim. Acta*, **70**, 227 (1983).

42) FEFF was developed for the calculation of solid materials. The Debye–Waller-like factor (σ) derived from FEFF using Debye temperature (Θ_D) corresponds to the atomic vibration of the phonon mode. If we substitute the IR vibrational frequency of the Hg–S stretching mode (N. Iwasaki, J. Tomooka, and K. Toyoda, *Bull. Chem. Soc. Jpn.*, **47**, 1323 (1974)) into the equation of Debye temperrature ($\Theta_D = h\omega_D/k_B$), we obtain $\Theta_D = 470$ K. It is a matter of course that this substitution has no physical meaning. In practice, σ of compound **1** was not simulated with $\Theta_D = 470$ K. However, it is possible to use Θ_D as a mediator for obtaining the ture σ of the first shell. The radial distribution of Hg–S at 295 K was best simulated by $\Theta_D = 575$ K, which afforded $\sigma = 0.061$ Å.

43) FEFF simulation was carried out for $SO^2 = 0.8$, 0.84, 0.87, 0.9, and 1.0. E. A. Stren, S. M. Heald, and B. Bunker, *Phy. Rev. Lett.*, **42**, 1372 (1979).

44) G. Wagner, W. Braun, T. F. Havel, T. Schaumann, N. Go, and K. Würtrich, *J. Mol. Biol.*, **196**, 611 (1987).

45) I. -J. L. Byeonand and M. Llinas, *J. Mol. Biol.*, **222**, 1035 (1991).

46) K. Würthrich, "NMR in Biological Research: Peptides and Proteins," North-Holland Publishing Co., Amsterdam (1976).

47) a) Y. V. Venkatachalapathi, V. V. Prasad, and P. Balaram, *Biochemistry*, **21**, 5502 (1982); b) A. Ravi, B. V. Venkataram Prasad, and P. Balaram, *J. Am. Chem. Soc.*, **105**, 105 (1983); c) B. N. N. Rao, A. Kumar, H. Balaram, A. Ravi, and P. Balaram, *J. Am. Chem. Soc.*, **105**, 7423 (1983); d) R. Kishore, H. Ishizaki, A. T. Tu, A. Ravi, and P. Balaram, *Int. J. Peptide Protein Res.*, **30**, 474 (1987); e) R. Kishore, S. Raghothama, and P. Balaram, *Biochemistry*, **27**, 2462 (1988).

48) T. E. Ferrin, C. C. Fuang, L. E. Jarvis, and R. Langridge, "The MIDAS Display System," *J. Kol. Graphics*, **6**, 13 (1988).

49) W. A. Gunsteren and H. J. C. Berendsen, *Mol. Phys.*, **34**, 1311 (1977).

50) G. D. Rose, L. M. Gierasch, and J. A. Smith, *Adv. Protein Chem.*, **145**, 215 (1985); C. Ghélis and J. Yon, "Protein Folding," Academic, New York (1982), p. 63.

51) See Ref. 1, p. 49.

52) to be published elswhere.